OPEN ACCESS

International
Journal
Of Modern Engineering Research (IJMER)

Investigation on An Impinging Square Jet

Rocco Mario Di Tommaso, *Enrico Nino
**(Scuola di Ingegneria*
University of Basilicata, ITALY)
*Corresponding Author: *Enrico Nino*

ABSTRACT: *This paper focuses on an impinging laminar square jet, experimental and numerical investigated, under several Richardson number conditions. The experimental measurements have been performed by means of a PIV (Particle Image Velocimetry) technique in order to infer the structure of a square single jet impinging on a heated flat plate, maintained at a constant temperature. The experiments have been carried out for jet Reynolds number between 250 and 400 and Richardson number between 0 (isothermal condition) and 0.8. The investigated jet-to-plate spacing was 0.3 L and 0.1 L, where L is the jet width. Numerical simulations using CFD software have been then performed, investigating numerically through the solution of the three-dimensional Navier-Stokes and energy equations in steady state.*

The obtained results show that: in the case of jet-to-plate distances H/L=0.1 the jet is substantially diverted in the transverse direction and the wall jet fills substantially the whole gap between the plate and the plenum in all the investigated Richardson number. In the case of H/L=0.3 the results are substantially different. In fact the buoyancy generated by the warm gas adjacent the warm plate are able to deviate the wall jet with the formation of coherent vortex depended of the adopted Reynolds number.

Keywords: *: CFD, Impinging Square Jet, PIV, Wall Jets.*

I. INTRODUCTION

Impinging jets have found a large number of applications where high rates of convective heat transfer are required. Industrial uses of impinging air jets include tempering of glass, drying of paper and textiles, and the cooling of the metal sheets, micro-electronic components, and turbine blades. Impinging jets are generally used to increase the rate of heat transfer between a fluid and solid, and are quite often employed to produce enhanced and controlled localized cooling or heating effects on surfaces, as compared with non-impinging flows. Although most of the applications of impinging jets are turbulent, the three-dimensional laminar flow structure resulting from a square jet is far from being fully understood. Laminar jets are also encountered when the fluid is viscous or the geometry is miniature as in microelectronics, or the velocity is low in order to have low mass flow rate. Although such jets yield very high heat transfer coefficients in the stagnation zone and the cooling performance drops rapidly away from the impingement zone.

The heat transfer process in an impinging jet may fall in the forced or mixed convection regime, depending on the Richardson number, Ri, which is the ratio of the Grashof number and the Reynolds number squared. If Ri << 1, the force convection process is dominant, whereas for dominant natural convection, Ri >> 1. In the case where Ri is of the order 1, force and natural convection are comparable and the process falls into the mixed convection regime. The interaction between the inertia or viscous force and the bouncy driven flows make the resulting heat transfer process very complex. Therefore, in many applications of an impinging confined jet the bouncy effects may be significant and can not be ignored. In such flow the mixed convection process must be considered for the heat transfer analysis.

Furthermore the wall jet after impingement produces a rather complex flow field, therefore, the study of three-dimensional impinging jet may provide some basic understanding. Numerous studies have been reported in the literature on the flow, heat and mass transfer distribution under single laminar impinging jets with considering force convection, without taking into account the bouncy effects. Gardon and Akfirat [1] carried out an early work to measure the heat transfer coefficients between a flat plate and impinging 2-D slot-jets. They focused on single jets and arrays of free air jets in laminar and turbulent flow conditions. Scholtz and Trass [2] investigated, both numerically and experimentally, the laminar impinging mass transfer with a non-uniform laminar velocity profile, for nozzle to plate spacing ranging from 0.05 to 6 nozzle diameters. They found that the impinging mass transfer was independent of the nozzle-to-plate spacing within the range of 0.5-6.0 nozzle diameters for 500<Re<1970. Chou and Hung [3] numerically investigated the effect of initial velocity profile at the nozzle exit on stagnation and

local heat transfer of a confined slot-jet normally impinging on an isothermally heated surface. The range of the Reynolds number, based on the width of the slot jet, used is from 100-400.

Elison and Webb [4] experimentally investigated fully developed liquid jets impinging normally on a constant heat flux surface. Their study focused on jet Reynolds number at the nozzle exit between 300-7000 and for jet-to-plate spacing from 1.5-20 jet diameters. Sezai and Mohamad [5] studied numerically the flow and heat transfer characteristics of impinging laminar jets issuing from rectangular nozzles of different cross sections.

There are very few reported studies in literature considering mixed convection effects in confined slot jets impingement. Sparrow and Minkowycz [6] studied bouncy-force effects on laminar force convection over a horizontal flat plate. Hieber [7] determined bouncy effects analytically for the laminar boundary layer region above an isothermally heated, semi-infinite horizontal surface located in a horizontal uniform stream. Yuan et al. [8], who found a substantial heat transfer enhancement for high Richardson number conditions, and jet offset peaks in the Nusselt number distribution. Wang et al. [9] investigated numerically a not confined circular jet impinging on a heated surface. They found that the Nusselt number is considerably influenced by natural convection only in the case of large difference between the initial gas temperature and the substrate temperature and at low Reynolds number, with detrimental effects on the heat transfer at the stagnation point. Potthast et al. [10] performed mixed convection simulations relative to confined axial or radial jet impingement. They found that free convection may influence the jet impingement on a horizontal plate by increasing the heat transfer, and obtained periodic solution for the smallest Grashof number and a chaotic flow for the largest Grashof number. Sahoo and Sharif [11, 12] investigated the associated heat transfer process in the mixed convective regime in a two dimensional model. The range of the Reynolds number and jet-to-plate spacing used are from 100-500 and from 2-5 respectively. The Richardson numbers varies between 0-10. They reported that the bouncy effects are not very significant in the overall heat transfer process for the range of Reynolds number considered in there study. More over the magnitude of the local Nusselt number is reduced as the jet-to-plate spacing increases.

The experimental investigation of single jet in laminar range with mixed convection is quite scarce. Several papers [13-17] are related with impingement of laminar slot jet which is two dimensional. Although, the work of Aldabbagh and Mohamad [18] are three dimensional but it is related to force convection, without taking into account the bouncy effects.

The present work deals with experimental bi-dimensional and numerical three-dimensional analysis of a square single jet impinging on a heated flat surface (Fig. 1). The flow field have been investigated by means of computational fluid dynamics (CFD) and Particle Image Velocimetry (PIV), which are performed under similar conditions. A series of velocity vectors and streamline graphs at different cross-sections are achieved in CFD simulation and PIV experiment to get better jet configuration. This study allows gaining better insight into the mechanism of airflow and the experimental data obtained will be used to validate the computational results. The structure of the generated flow field was investigated (both numerical and experimental) for Reynolds number ranging from 250-400, Richardson number ranging from 0 to 0.8 and H/L sets at the value of 0.1 and 0.3.

II. EXPERIMENTAL SET-UP

The experimental investigations have been performed on a simple nozzle with a square cross section, realized directly on the wall of the plenum, with a lateral dimension L = 0.01 m. Below the plenum a metal (steel) plate is opportunely positioned in order to realize a H/L ratio of 0.1 and 0.3. An electrical heater, drive by means of an adjustable transformer, increase the metal plate temperature at a value as high as 55°C, in order to reach a maximum Ri of 0.8 at Re = 250.

A PIV system has been employed to analyze the instantaneous behavior of the velocity field. The adopted system (whose layout is visible in fig. 1) is based on two pulsed Nd:YAG lasers firing on the second harmonic (green 532 nm). The beams, properly separated in time, are recombined on the same optical path by means of a polarized dichroic filter. Then the beams are expanded in one direction, by means of a combinations of spherical (negative) and cylindrical lens, in order to obtain a 70 mm wide and 0.3 mm thick laser sheet in the measuring region. The laser sheet is used to illuminate the airflow over the nozzle. An aerosol generator has been used in order to seed the gaseous flow with small droplets of distilled water.

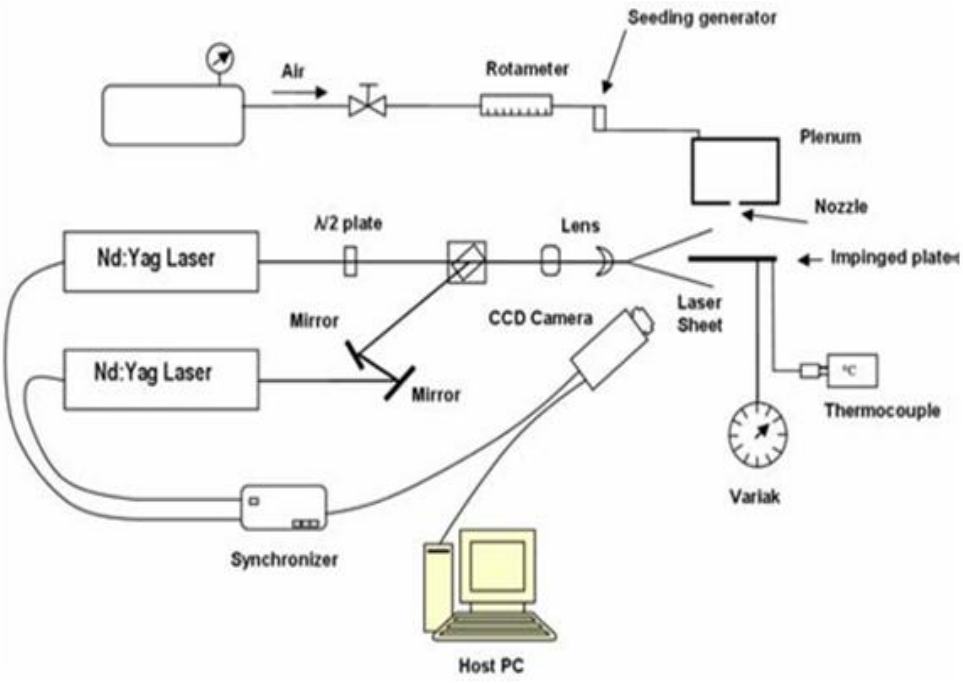

Fig. 1. Experimental set-up

The images have been collected by of a double frame 1280 x 1024 pixels PCO CCD camera synchronized with the two laser beams and with the frame grabber by means of a dedicated electronic synchronizer. The images are formed by two different layers, each of them containing information about the seeding positions obtained by firing one of the two lasers. So the initial seeding positions (first laser beam, image on the first layer) and the final one (second laser beam, image on the second layer) is spotted.

The images were then post-processed by means of the TSI Insight V.3.2 software in order to extract the sub-images formed by 32 X 32 pixels from each layer, and to perform a cross-correlation between the two corresponding sub-images. An interrogation algorithm extracts the correlation peak position from the cross-correlation domain with a sub-pixel precision, and performs the calculation of the two velocity components for those sub-images, by means of a pixel-to-mm conversion factor. Interrogations are repeated using a recursive algorithm for the entire set of double frames images. The measured velocities are reported in a grid with size of 32 x 32 pixels with a 50% overlap (Nyquist criteria). The two laser beams have been fired at about 100 mJ per pulse (second harmonic), and with separation time of 90 ms. The measurement volume has been stretched up to 1 mm from the impinged plate. The overall estimated error has been evaluated, according to [19 to 21], as about 4% on Vav.

III. NUMERICAL MODEL

In this work, CFD software FLUENT was employed to simulate the fluid flow distribution. FLUENT is one of the most widely used commercial codes for simulating engineering fluid flow due to its accuracy, robustness and convenience. In FLUENT, the conservation equations of mass, momentum are solved using the finite volume method [22].

There are some assumptions in the CFD simulation: the flow is stable in the test section; the fluid flow meets the Boussinesq assumption and the fluid in the test section is incompressible Newtonian fluid.

The steady-state, three-dimensional, Navier-Stokes and energy equations for incompressible flows in Cartesian coordinates are used for this study. The velocity and length are adimensionalized by jet-exit velocity and jet width, respectively.

With airflow is in transition toward turbulent regime the usual turbulent models (RANS, Reynolds averaged Navier Stokes) are not well adapted for transition regime. Therefore, laminar flow assumption was made for the flow regime in our simulation and transient resolution was used (with sensibility study of time step) allowing the capture of certain unsteady characteristic. Boussinesq approximation was used since the air temperature variation is small compared with the mean absolute value.

The dimensionless continuity, momentum and energy equations for laminar flow with constant properties can be written as:

$$\frac{\partial U}{\partial X}+\frac{\partial V}{\partial Y}+\frac{\partial W}{\partial Z}=0$$

$$U\frac{\partial U}{\partial X}+V\frac{\partial V}{\partial Y}+W\frac{\partial W}{\partial Z}=-\frac{\partial P}{\partial X}+\frac{1}{\mathrm{Re}}\nabla^2 U$$

$$U\frac{\partial U}{\partial X}+V\frac{\partial V}{\partial Y}+W\frac{\partial W}{\partial Z}=-\frac{\partial P}{\partial Y}+\frac{1}{\mathrm{Re}}\nabla^2 V$$

$$U\frac{\partial U}{\partial X}+V\frac{\partial V}{\partial Y}+W\frac{\partial W}{\partial Z}=-\frac{\partial P}{\partial Z}+\frac{1}{\mathrm{Re}}\nabla^2 W$$

$$U\frac{\partial U}{\partial X}+V\frac{\partial V}{\partial Y}+W\frac{\partial W}{\partial Z}=\frac{1}{\mathrm{Re}\,\mathrm{Pr}}\nabla^2 T$$

Boundary conditions for velocities: the outlet boundary is located far enough downstream for conditions to be substantially developed, accordingly the following conditions are imposed:

$$\frac{\partial U}{\partial X}=\frac{\partial V}{\partial X}=\frac{\partial W}{\partial X}=0 \qquad \text{at X=3L , X=-3L}$$

$$\frac{\partial U}{\partial Y}=\frac{\partial V}{\partial Y}=\frac{\partial W}{\partial Y}=0 \qquad \text{at Y=3L , Y=-3L}$$

All walls are stationary therefore the no-slip boundary condition is used for the top and bottom solid walls except the W velocity at the jets exit cross-section at the top wall, where it was set to be equal to unity and, hence, U = V = W = 0 at Z = 0, Z = H/L except at nozzle exit, U = V = 0, W = —1 at nozzle exit.
Boundary conditions for temperature are as follows: if the fluid exits the domain the first derivative of temperature is set to zero and if the fluid flows from the surroundings into the domain then the fluid temperature is set to surrounding temperature. That is:

$$\text{At X=-3L}\quad \begin{cases} \dfrac{\partial T}{\partial X}=0 & for\ \ U<0 \\ T=0 & for\ \ U>0 \end{cases}$$

$$\text{At X=3L}\quad \begin{cases} \dfrac{\partial T}{\partial X}=0 & for\ \ U>0 \\ T=0 & for\ \ U<0 \end{cases}$$

$$\text{At Y=-3L}\quad \begin{cases} \dfrac{\partial T}{\partial Y}=0 & for\ \ V<0 \\ T=0 & for\ \ V>0 \end{cases}$$

$$\text{At Y=3L}\quad \begin{cases} \dfrac{\partial T}{\partial Y}=0 & for\ \ V>0 \\ T=0 & for\ \ V<0 \end{cases}$$

Adiabatic boundary conditions are imposed on the top wall, except at the nozzle exit cross-section where temperature was set to be equal at ambient (and jet) temperature. The bottom wall is set to a higher temperature than the ambient,

At Z=0 T = 1

$$\text{At Z= H/L} \quad \frac{\partial T}{\partial Z} = 0 \quad \text{except at nozzle exit}$$
$$T = 0$$

The adopted thermal boundary conditions, based on uniform global heat transfer coefficient between external air and heated surface, have been set as: Constant external air temperature (20 °C); Constant heated surface temperature (Ri).

Iterations are continued until the second norm of the residuals for all equations are reduced below 10^{-6}, where no significant variations have been observed.The cross-section of the nozzles is taken to be square and the velocity distribution at the exit of the nozzles is assumed uniform with a flat profile.Transient simulation was performed and only the results obtained after the convergence was taken into account. Sixty numerical velocity fields were saved every 250 ms and then the mean of these 60 velocity fields was used to compare with the average experimental values (also obtained from 60 pairs of PIV measurements).

III.1 MESH

Structured mesh were been used to describe the geometry of the impinging jet. Finer meshes were used near walls in order to accurately describe the fluid dynamic and thermal boundary layers. The total number of cells adopted was 30965, mesh structure is shown in Fig. 2. To ensure that the results were not influenced by the cell numbers of the mesh, a sensitivity study was previously carried out.

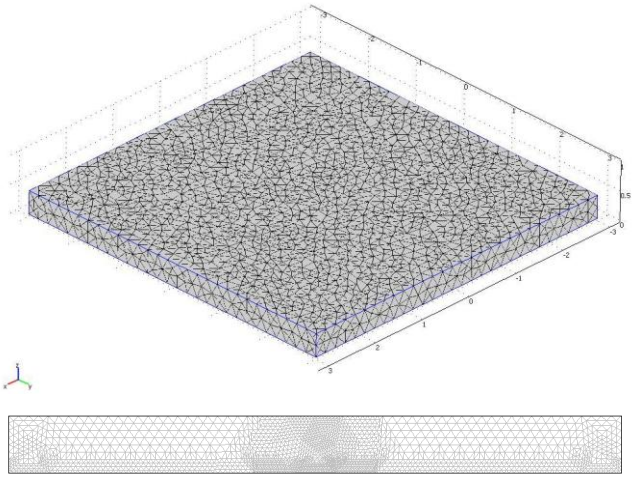

Fig. 2 Total 3D and 2D (section) mesh visualization

IV. RESULTS AND DISCUSSION

The results experimentally (PIV) obtained and numerically predicted (CFD) are reported by means of path lines, images, velocity magnitude and distribution. The investigated conditions are reported in Tab. 1.

Isothermal		Plate temperature T= 55°C		
H/L	*Re*	*H/L*	*Re*	*Ri*
0.1 and 0.3	250	0.1 and 0.3	250	0.70
0.1 and 0.3	300	0.1 and 0.3	300	0.49
0.1 and 0.3	350	0.1 and 0.3	350	0.35
0.1 and 0.3	400	0.1 and 0.3	400	0.27

Table 1. Experimental conditions investigated

A first comparison can be made under isothermal conditions (*Ri*=0). The impinging jet show the usual behavior of a not confined jet generated by a circular nozzle [13]. In fact velocity distribution, measured in a symmetric axial plane (Fig. 2 and 3) show the stagnation region positioned just below the nozzle, the lateral acceleration and recirculation region were positioned around the nozzle exit. This behavior is clear visible in the case of *H/L* = 0.3 for both PIV measurement (Fig. 2) and CFD simulation (Fig. 3). So the expected behavior [18] of a jet filling the whole channel is not confirmed, at least for *Re* as high as 300 and *H/L* around 0.3.

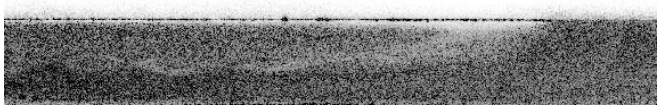

(A)

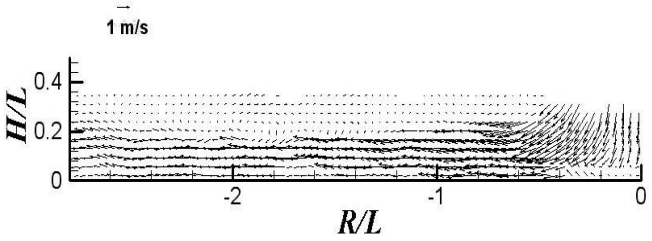

(B)

Fig. 2. PIV image (A) and velocity distribution (B) at *H/L*=0.3, *Re*=400, and *Ri* =0

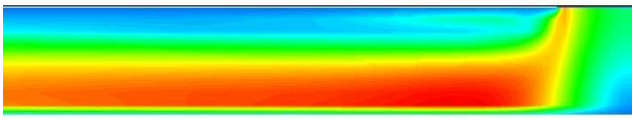

(A)

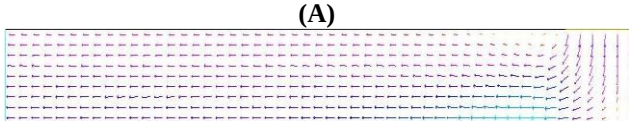

(B)

Fig. 3. CFD velocity magnitude contours (a) and velocity distribution (b) at *H/L*=0.3, *Re*=400, and *Ri* =0

Increasing the temperature of the impinged plate (i.e. increasing the *Ri* number) the behavior of the impinging jet change remarkably. As it is possible to see in Fig. 4, in which a gaseous oscillation is visible just in the middle of the gap (confining channel) formed by the impinged plate and the plenum wall in which the nozzle is realized. In practice with a *Ri* number different from zero, the gaseous jet is flowing between the warm gas, adjacent the impinged surface, and the practically stagnant gas in the upper zone of the channel. This effect, present even for *Ri* as high as 0.8 start to grow up in the case of *Ri* = 0.27, with the formation of consistent coherent vortices, as visibly in Fig. 5. The same effect has been found in the CFD simulation reported in Fig. 6A (PIV image) and Fig. 6B (CFD results). At the increase of *Ri* number, the lateral jet's detachment begin at a R/L as low as 0.5 and it is a little bit more pronounced than the previous case, as visible in Fig.7.

(A)

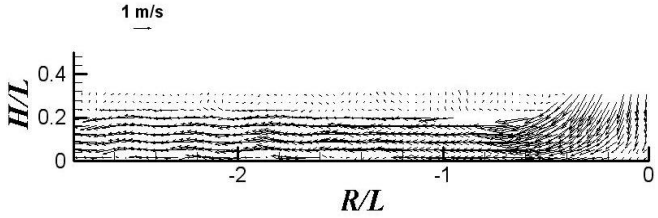

(B)

Fig. 4. PIV image (A) and velocity distribution (B) at *H/L* =0.3 *Re* =400 and *Ri* =0.27.

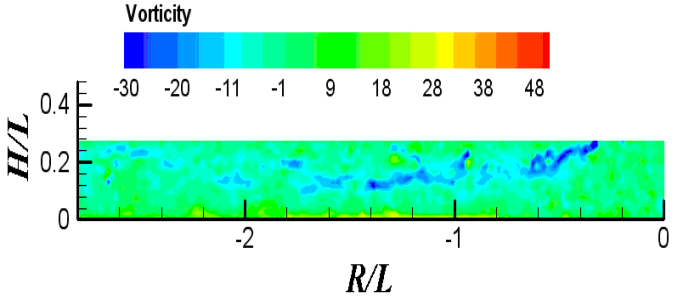

Fig. 5. Vorticity distribution at *H/L* =0.3 *Re* =400 and *Ri* =0.27

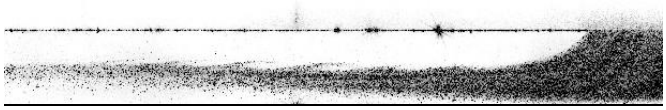

(A)

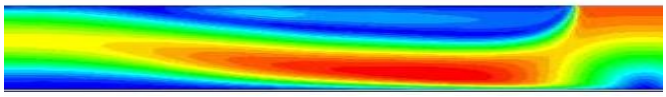

(B)

Fig. 6. PIV image (A) and CFD velocity distribution (B) at *H/L* =0.3, *Re* =350 and *Ri* =0.35.

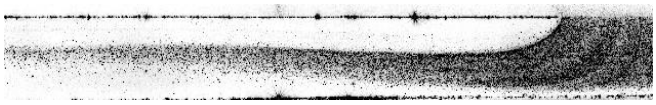

(A)

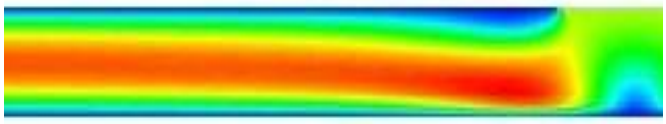

(B)

Fig. 7. PIV image (A) and CFD velocity distribution (B) at *H/L*=0.3, *Re* =300 and *Ri* =0.49.

A different effect was observed in the case of *H/L* as low as 0.1 and *Ri* = 0.27. In this configuration the channel height is substantially comparable with the amplitude of the vortex measured in the condition of the image reported in Fig. 4, so the coherent vortex was not observed and the lateral jet is forced to flow without surfaces instability (vortex), filling substantially the whole channel (Fig. 8A). The same effect was observed also in the CFD simulations (Fig. 8B).

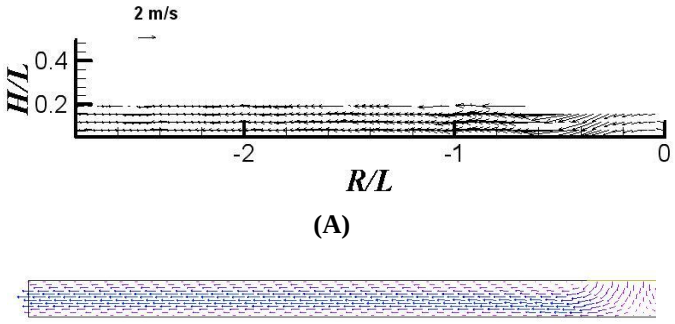

(A)

(B)

Fig. 8. PIV image (A), velocity distribution (B) and CFD vectorial field at H/*L* =0.1, *Re* =400 and *Ri* =0.27.

In order to highlight the agreement between PIV and CFD results, velocity magnitude plot, in a chromatic scale, are reported in Fig. 9. In this figure a detail of the high speed deflection region show a consistent agreements between the results obtained by the two techniques. In particular the CFD results (Fig. 9B) show a little bit more velocity details compared with the velocity magnitude distribution experimentally measured (Fig. 9A). The differences was probably caused by the low-pass filter effect induced by the seeding. The same effect is visible in Fig. 10, in which the path lines distributions (obtained under the same conditions of the previous figure) are reported. In this case the two results are quite different, but in the case of experimental results the upper left region show a substantial absence of velocity distribution, caused by a very low seeding density. In effect we seed the main stream directly in the plenum. That means that in some regions of the flow field (like the upper left region of Fig 9A) the seeding density is not enough to produce reasonably good measurements. It is obvious that in CFD simulation this kind of problems are avoided and in the upper left region of Fig. 9B we observe a significant distribution of path line.

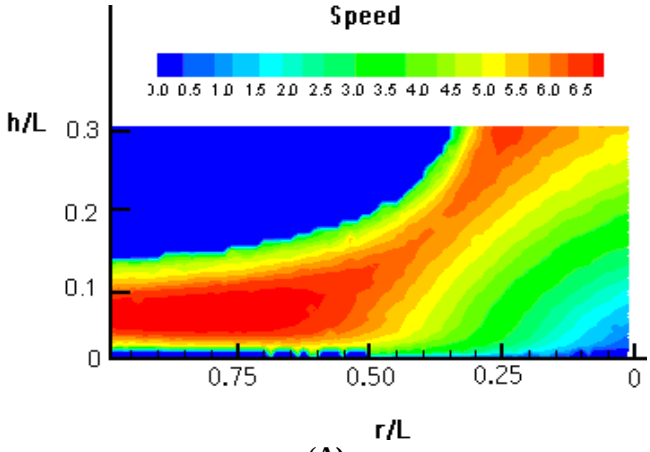

(A)

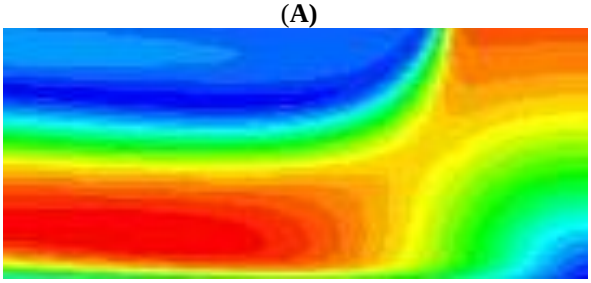

(B)

Fig. 9 Comparison between experimental (A) and numerical (B) velocity magnitude *H/L* =0.3, *Re* =400, *Ri*=0.18

The good agreement between experiments and simulations is comforted, also, by the observation of the maximum velocity measured and calculated. In fact, this two value are similar, with a maximum measured value of 7,3 m/s and a maximum predicted value of 7,6 m/s.

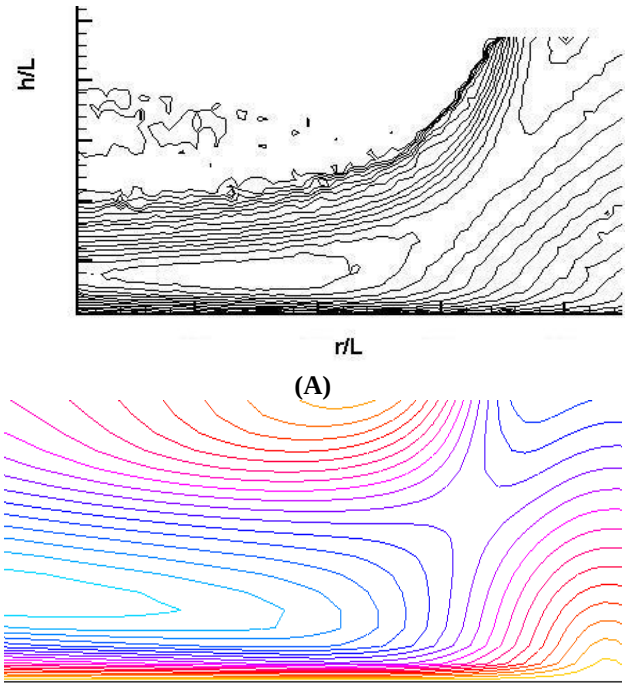

Fig. 10. Comparison between experimental (A) and numerical (B) path lines *H/L* =0.3, *Re* =400 and *Ri*=0.18

V. CONCLUSION

Experimental measurements with PIV technique and 3D numerical CFD simulations have been performed in order to determine the flow characteristics of impinging jet generated by a nozzle with a square cross-section. The experiments and computations, performed under similar conditions, have been focalized on the effect of the *Ri* number on flow field generated, at the variation of *Re* number and for two *H/L* conditions.Relatively good agreement between measured and calculated airflow profiles have been obtained. The results indicate that for the lowest investigated aspect ratio (*H/L* = 0.1), the structure of the generated flow is moderately affected by the Richardson number in all the Reynolds number investigated. Moreover the wall jet fill substantially all the channel formed by the impinged plate and the plenum.

In the case of *H/L* = 0.3 the influence of the *Ri* number is remarkably, specially at the increase of the Reynolds number. In particular, with a *Ri* different from zero, the buoyancy effect, due to the warm air near the impinged plate, is able to deviate the wall jet. With a Reynolds number as high as 400 the wall jet is clearly destabilized with the formation of several coherent vortices. The wall jet detachment is substantially well predict by the CFD simulations as well as the magnitude of the maximum velocity. Some discrepancies, between experiment and numerical results, have been fond in the velocity details around the wall jet, specially at *H/L*=0.3. In this conditions the plate to plate gap was not fill completely by the wall jet, allowing the formation of coherent structures (vortex). In the case of *H/L*=0.1 the wall jet fill completely the gap and less discrepancies, between PIV an CFD results, have been observed. Finally below the nozzle the stagnation region do not appear influenced by the *Ri* number in all the configurations investigated.

REFERENCES

[1]. R. Gardon, J. C. Akfirat, Heat transfer characteristics of impinging two dimensional air jets, J. Heat Transfer (1966) 101-108.

[2]. M. T. Scholtz, O. Trass, Mass transfer in a nonuniform jet: Part 2. Boundary layer flow mass transfer, AICHE J. 16 (1970) 90-96.

[3]. Y. J. Chou, Y. H. Hung, Impingement cooling of an isothermally heat surface with a confined slot jet, J. Heat Transfer 116 (1994) 479-482.

[4]. B. Elison, B. W. Webb, Local heat transfer to impinging liquid jets in the initially laminar, transitional, and turbulent regimes, Int. J. Heat Mass Transfer 37 (1994) 1207- 1216.

[5]. I. Sezai, A. A. Mohamad, 3-D Simulation of laminar rectangular impinging jets, flow structure and heat transfer, ASME Journal of Heat Transfer 121 (1999) 50-56.

[6]. E. M. Sparrow, W. J. Minkowycz, Buoyancy effects on horizontal boundary-layer flow and heat transfer, Int. J. Heat Mass Transfer 5 (1962) 505-511.
[7]. C. A. Hieber, Mixed convection above a heated horizontal surface, Int. J. Heat Mass Transfer 16 (1973) 769-772.
[8]. T. D. Yuan, J. A. Liburdy, T. Wang, Buoyancy effects on laminar impinging jets, ASME J. Heat Transfer, No. 31, 10 (1988) 2137-2145.
[9]. Y. B. Wang, C. Chaussavoine, F. Teyssandier, Two-dimensional modeling of a nonconfined circular impinging jet reactor-fluid dynamics and heat transfer, Int. J. Heat Mass Transfer 36 (1993) 857-873.
[10]. F. Potthast, H. Laschefski, N. K. Mitra, Numerical investigation of flow structure and mixed convection heat transfer of impinging radial and axial jets, Numer. Heat Transfer, Part A 26 (1994) 123-140.
[11]. D. Sahoo, M. A. R. Sharif, Mixed convective cooling of an isothermal hot surface by confined slot jet impingement, Numer. Heat transfer, Part A 45 (2004) 887-909.
[12]. D. Sahoo, M. A. R. Sharif, Numerical modeling of slot-jet impingement cooling of a constant heat flux surface confined by a parallel wall, Int. J. of Thermal Sciences 43 (2004) 877-887.
[13]. M. Angioletti, R.M. Di Tommaso, E. Nino and G. Ruocco "Simultaneous Visualization of Flow Field and Evaluetion of Local Heat Transfer by Transitional Impinging Jets", Int. J. Heat Mass Transfer, 46 (2003) 1703 – 1713, ISSN 0295-5075.
[14]. Di Lorenzo, Giuseppe & Manca, Oronzio & Nardini, Sergio & Ricci, Daniele. (2012). Numerical Study of Laminar Confined Impinging Slot Jets with Nanofluids. Advances in Mechanical Engineering. 2012. 248795. 10.1155/2012/248795.
[15]. F.J. Hong, C.Y. Zhang, W. He, P. Chenga, G. Chen. Confined Jet Array Impingement Boiling of Subcooled Aqueous Ethylene Glycol Solution. International Communications in Heat and Mass Transfer 56 (2014) 165–173.
[16]. Dae Hee Lee, Seong Jung Kim, Young Hwan Kim, Hyun Jin Park. Heat Transfer With Fully Developed Slot Jets Impinging on Confined Concave and Convex Surfaces. International Journal of Heat and Mass Transfer 88 (2015) 218–223
[17]. El-Maghlany, W., et al.: Premium Jet Cooling with Two Ribs over Flat Plate Utilizing Nanofluid Mixed Convection. THERMAL SCIENCE, Year 2017, Vol. 21, No. 2, pp. 963-976
[18]. Aldabbagh, Loay & Mohamad, Abdulmajeed. (2009). Mixed Convection in an Impinging Laminar Single Square Jet. Journal of Heat Transfer-transactions of The ASME - J HEAT TRANSFER. 131. 10.1115/1.3000970.
[19]. M. Ra.el, C. Willert, J. Kompenhans, Particle Image Velocimetry, Springer, Berlin, 1998.
[20]. R. Kean, R.J. Adrian, Optimization of particle image velocimeters—Part 1. Double pulsed systems, Meas. Sci. Technol. 1 (1990) 1202–1215.
[21]. U. Ullum, J.J. Schmidt, P.S. Larsen, D.R. McCluskey, Statistical analysis and accuracy of PIV data, in: Proceedings of the 2nd International Symposium on PIV, Fukui, Japan, 9–11 July 1997.
[22]. FLUENT Computational Fluid Dynamic Code Version 6.3 User Guide, Fluent Inc., http://www.fluent.com/

*Enrico Nino. "Investigation on An Impinging Square Jet" International Journal Of Modern Engineering Research (IJMER), vol. 07, no. 10, 2017. 05-14